Structural, Electronic and Transport Properties of Hybrid $SrTiO_3$-Graphene and Carbon Nanoribbon Interfaces

Jakub D. Baran[1], Christopher Eames[1], Keisuke Takahashi[2,3], Marco Molinari[1,4], M. Saiful Islam[1] and Stephen C. Parker[1,*]

[1]*Department of Chemistry, University of Bath, Claverton Down, Bath BA2 7AY, UK*
[2]*Center for Materials Research by Information Integration (CMI[2]), National Institute for Materials Science (NIMS), 1-2-1 Sengen, Tsukuba, Ibaraki 3 05-0047, Japan*
[3]*Graduate School of Engineering, Hokkaido University, N-13, W-8, Sapporo 060-8628, Japan*
[4]*Department of Chemistry, University of Huddersfield, Huddersfield, HD1 3DH, U.K.*

*Corresponding author: S.C.Parker@bath.ac.uk

Abstract

Hybrid materials composed of different functional structural units offer the possibility of tuning both the thermal and electronic properties of a material independently. Using quantum mechanical calculations, we investigate the change of electronic and thermoelectric transport properties of graphene and hydrogen terminated carbon-nanoribbons (CNR) when these are placed on the $SrTiO_3$ (001) surface (STO). We predict that both *p-type* and *n*-type composite materials can be achieved by coupling graphene/CNR to different surface terminations of STO. We show that the electronic properties of graphene and CNR are significantly altered on SrO-terminated STO but are preserved upon interaction with TiO_2-terminated STO and that CNRs possess distinct electronic states around the Fermi level due to their quasi-one-dimensional nature, leading to a much higher calculated Seebeck coefficient than that of a pristine graphene sheet. Moreover, our calculations reveal that in the TiO_2-$SrTiO_3$/CNR system there is a favourable electronic level alignment between the CNR and STO, where the highest occupied molecular orbital of the CNR is positioned in the middle of the STO band gap, resembling *n*-type doping of the substrate. Our results offer design principles to guide the engineering of future hybrid thermoelectric materials and, more generally, nano-electronic materials comprising oxide and graphitic components.

1. Introduction

Many approaches have been tried to improve the thermoelectric properties of materials. Among these are doping[1], nano-engineering[2, 3] or dimensionality reduction[4]. However, despite decades of extensive research, applications of thermoelectric devices composed of earth abundant and non-toxic materials are still limited. The figure of merit for a thermoelectric material is $ZT=S^2\sigma T/(k_e+k_l)$ with S being a Seebeck coefficient, σ being the electronic conductivity, T being temperature, k_e and k_l being thermal electronic and phonon conductivity. High values of ZT are difficult to obtain because the component variables are very difficult to control independently. This originates from the fact that all but k_l are related to the electronic structure of a material and are therefore interdependent. For example, increasing the Seebeck coefficient decreases the electronic conductivity and *vice versa.*[2] Previous improvements in ZT have been due to selecting materials based on a careful consideration of their electronic and thermal properties and are mostly related to bulk three-dimensional cases. The next logical step is to make materials modular, where each module plays a distinct role. Such hybrid materials can be thought as combinations of building blocks with different electrical and thermal properties. Thus, by selectively choosing individual components, with distinct electronic and thermal properties, a material with desired properties that are not exhibited by any of the bulk components could in principle be achieved.[5] Two-dimensional multilayer systems are the simplest example of hybrid materials and so far have not been investigated to the same extent as the bulk materials. These thin film systems are of increasing importance due to constant miniaturisation of electronic components and advances in nano-scale fabrication that enable tailoring of their properties.[6]

The physics and chemistry at the interface between different material components dominate the electronic properties of the overall system. At the atomic-scale, the interaction between different parts of a hybrid material involves bond rehybridization and charge transfer, which modifies the electronic transport properties, e.g., electronic conductivity or Seebeck coefficient. In addition, modular design enhances phonon scattering, which results in a reduced thermal conductivity.[2] The fundamental challenge for hybrid thermoelectrics and nano-electronic materials is to find the composite materials that result in the desired efficiency and properties of the overall device. To address this challenge an effective strategy is required to identify suitable modular components.

One such class of modular materials are oxides, whose electronic structure is well understood and

can be readily controlled. $SrTiO_3$ has a large carrier effective mass resulting in a high Seebeck coefficient, good thermal stability at high temperature and strong structural tolerance for substitutional doping.[1] However, its application as thermoelectric materials is currently limited by a high operating temperature of >700C.[7] Another modular material that is particularly interesting from both from the fundamental point of view and due to its technological relevance is graphene and its derivatives. It has been recently shown that the thermal operating window of STO can be reduced to room temperature by the addition of graphene nano-flakes during preparation.[8] The unusual band structure of graphene gives rise to a variety of intriguing electrical and thermal phenomena.[9] Among them are remarkable electronic transport properties, such as a record carrier mobility of ~$2x10^5$ $cm^2V^{-1}s^{-1}$ and a Seebeck coefficient (*S*) of ~80 μVK^{-1}.[10, 11] However, due to its extremely high thermal conductivity (*k*) of 2-$5x10^3$ W/m[12-14] its overall ZT at a room temperature of ~0.01[10-12] is at least two orders of magnitude below that of leading thermoelectric materials.[2] Despite the extremely high thermal conductivity of graphene, it has been shown that addition of graphene nano-flakes to the STO reduces the thermal conductivity of STO.[8] Due to the system size (see Methodology section below), first principle calculations of the lattice thermal conductivity are computationally prohibitive for us at present. However, it has been recently shown that introduction of patterns on the graphene by its functionalization reduces thermal conductivity while keeping the power factor and electronic conductivity high, resulting in a predicted ZT of 3 at room temperature.[15] Chen *et al.*[16] showed that in case of the graphene/h-BN interface the overall superlattice thermal conductivity was decreased by 83% when compared with those of the parent materials, which indicates that construction of superlattice structures may be efficient method of decreasing lattice thermal conductivity of graphene. In the work of Yeandel *et al.*[17] it is shown that by nanostructuring $SrTiO_3$ a lower thermal conductivity over broad range of temperatures can be achieved. Even more interesting electronic properties can be found in elongated strips of graphene with a finite width such as carbon nanoribbons (CNRs). CNRs can be either metallic or semiconducting depending on the crystallographic direction of the ribbon axis and may present unique magnetic properties.[18] Moreover, due to technical advances, they can be produced in a highly controllable manner, which opens up great opportunities for the future design of such hybrid nano-materials.[19-22]

Here, we will focus on the structural, electronic and thermoelectric transport properties of pristine graphene and CNR and their interfaces with the STO surface. We will discuss the nature of interactions at the STO/Graphene(CNR) interface and how this affects the electronic and transport properties of the

composite system. First, we outline the computational methodology and following this we report the structural and electronic properties of graphene and CNR interfaces with TiO_2- and SrO- terminated (001) $SrTiO_3$ (STO) surfaces. Finally, we discuss the thermoelectric transport properties for these interfaces and compare them to the free graphene sheet and CNR.

2. Methodology

2.1. Interface design

For STO bulk, pristine graphene and CNR, 8x8x8, 14x14x1 and 4x14x1 the Monkhorst-Pack *k*-mesh were used. In case of the single layer of graphene and CNR a thick vacuum layer of 20 Å was used and a dipole correction along the surface normal was applied. The electronic convergence was $1x10^{-8}$ eV, and the force on each atom was optimised to less than $1x10^{-3}$ eV/Å. These settings result in calculated lattice constants of 3.949 and 2.460 Å for STO bulk and graphene, respectively, in good agreement with previous studies.[23] Here we use hydrogen terminated zigzag CNR, with a width of 3 and length 1 unit cell, see Fig 1d. The choice of the zigzag CNR was dictated by its excellent epitaxial match to the STO surface as discussed below.

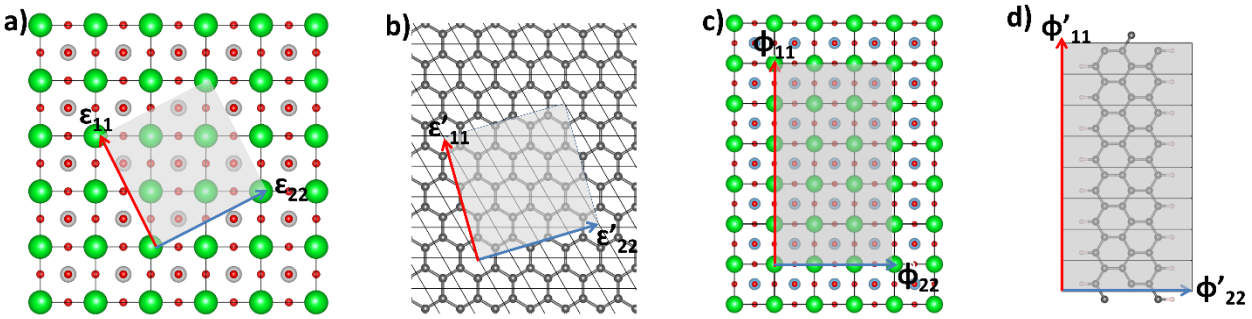

Figure 1: Lattice vectors of a) STO and b) graphene sheet in xy plane that were matched to create STO/Graphene interface. Similarly, lattice vectors of c) STO and d) CNR that were matched to create STO/CNR interface. Colour code: dark grey – C, blue – Ti, green – Sr, red – O, white – H. Solid black lines indicate lattice vectors of the primitive unit cell.

To model the interfaces, the lattice vectors of the STO and graphene/CNR were redefined as shown in Fig. 1a-d in order to find the best compromise between system sizes and mean absolute strain between the two components. For the STO/Graphene interface, the graphene sheet is strained by 0.42% along the ε'_{11} vector and 0.35% along the ε'_{22} vector (Fig. 1b) and then matched with the ε_{11} and ε_{22} unit cell vectors of the STO surface, which results in a mean absolute strain of 0.90%. Similarly, in the case of STO/CNR interface the CNR of 8x3 periodicity has been matched to the 3x5 STO surface (Fig. 1c-d), which resulted in stretching the CNR of 0.35% along ϕ'_{11}. We performed a potential energy surface scan

in order to determine the lateral position of the CNR on STO. The scan was performed with steps of $0.05\phi_{11}$ and $0.01\phi_{22}$, which resulted in 36 different configurations. All atoms were fully relaxed in this process. The $SrTiO_3$ (001) surfaces consist alternating TiO_2 and SrO (001) layers, and thereby can have two possible terminations, either TiO_2-terminated (hereafter referred to as Ti-STO) or SrO-terminated (hereafter referred to as Sr-STO).[24] In this work an 11 molecular layers thick slab of STO was used, and both non-stoichiometric surfaces with TiO_2/TiO_2 and SrO/SrO termination at both ends, as well as stoichiometric with TiO_2/SrO terminations were considered. However, due to difficulties in the separation of electronic contributions from the TiO_2 and SrO terminated surface within the same slab for the stoichiometric compositions, we will consider only the non-stoichiometric terminations here. A vacuum layer of 20 Å and a dipole correction along the surface normal was applied.

2.2. Geometry Optimization

The ground state atomic and electronic structure was calculated with first-principles density functional theory, using the plane-wave DFT code VASP.[25-27] Core electrons were represented by PAW pseudopotentials.[28] Electron exchange and correlation interactions were accounted for by the PBE exchange-correlation functional[29] and dispersion interactions by the inclusion of the Grimme D3 correction.[30] The plane-wave cut-off energy was 500 eV and the Monkhorst-Pack *k*-mesh was 4x4x1 and 4x2x1 for geometry optimisation for the STO/Graphene and STO/CNR systems, respectively. Electronic degrees of freedom have been converged to $1x10^{-6}$ eV. We have extensively tested the electronic smearing parameters to correctly describe the electronic properties of the free graphene (metallic) and CNR (semiconducting) and chose the Methfessel-Paxton method with a width of 0.15 eV for the free graphene and STO/Graphene interface and Gaussian smearing with a width of 0.1 eV for the free CNR and STO/CNR interface.

2.3. Boltzmann Transport Calculations and Electronic Density of States

The transport properties were calculated using the Boltzmann transport equation as implemented in the BoltzTraP code.[31] For this purpose, the Kohn-Sham eigenenergies were calculated on a very dense 24x24x1 *k*-point mesh for the free graphene and STO/Graphene interface and 16x8x1 *k*-point mesh for the free CNR and STO/CNR interface. These settings were also used to evaluate the electronic density of states (DOS). The transport calculations are carried out as a function of temperature and chemical

potential employing the constant relaxation time (τ) approximation (CRTA), which neglects the weak energy dependence of τ but recovers some doping and temperature dependence.[31] The CRTA methodology has been successfully applied to graphene/CNR[32] and oxide thermoelectric materials.[33-35] Within this methodology, τ is exactly cancelled in the expression of the Seebeck coefficient and thus can be directly evaluated from the first-principles band structure. While the thermopower can be obtained without any adjustable parameters using the CRTA, the evaluation of the electronic conductivity σ and the electronic part of the thermal conductivity requires knowledge of τ. Since the first-principles calculations do not give the actual scattering time, we will discuss here only $\sigma*\tau^{-1}$.

3. Results and discussion

3.1. Structural parameters of STO/Graphene and STO/CNR interfaces.

First, we report the energetic and structural properties of the interfaces. It has been reported that the surface energy of Ti- and Sr-terminated STO surfaces is almost the same[17] and, since both could co-exist, we investigate adsorption of graphene and CNR on both surface terminations. The atomic structure of the optimised interfaces is shown in Fig 2.

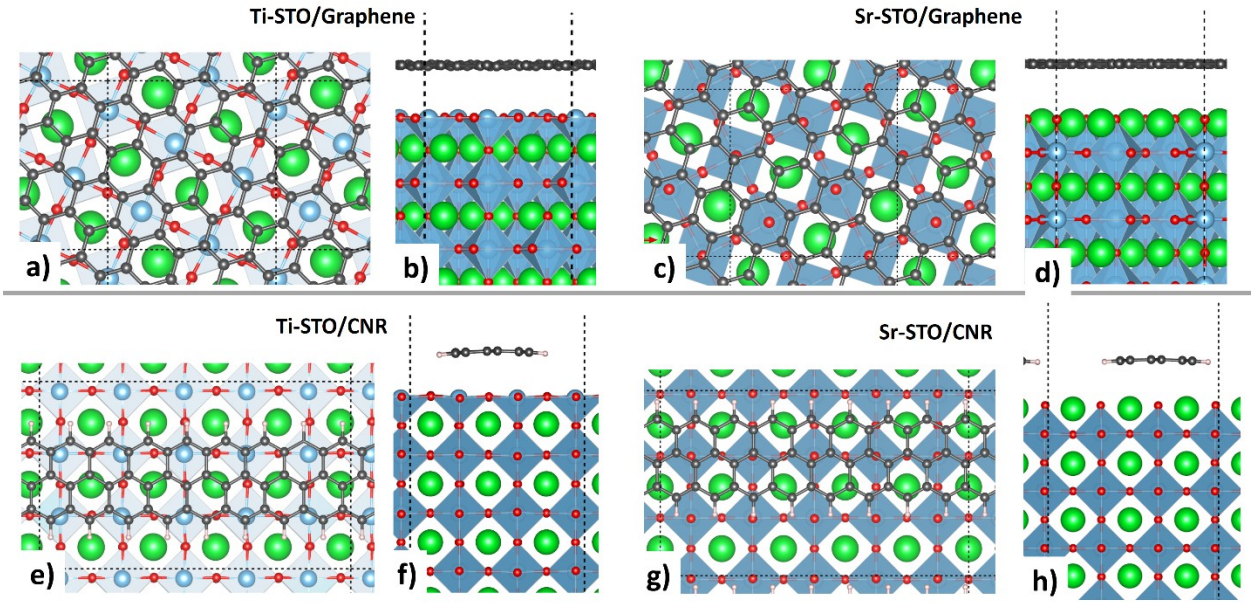

Figure 2: Atomic structure of interfaces between graphene or carbon nanoribbons with $SrTiO_3$ (001) surface viewed from above and side. (a-b) Graphene on Ti-terminated surface (c-d) graphene on Sr-terminated surface. (e-f) CNR on Ti-terminated surface (g-h) CNR on Sr-terminated surface. Colour code: dark grey – C, blue – Ti, Green – Sr, red – O, white – H.

Two key results emerge from the calculations. First, CNRs have higher adsorption energy than graphene and adsorb at a smaller separation from the surface. Second, it is more energetically favourable for both graphene and CNR to adsorb onto the Sr-terminated (001) surface rather than the Ti-terminated (001) surface. A further observation is the structural distortions in the graphene and CNR. The rumpling of the graphene sheet is negligible, with a standard deviation from perfect flatness of 0.036 and 0.004 Å for the Ti- and Sr- terminated STO, respectively. However, for both Ti- and Sr-terminated STO, the CNR edge aligns with the rows of the surface oxygen atoms as shown in Fig. 2e and 2g, resulting in a buckling of the CNR (Fig. 2f and Fig. 2h) by 0.3 Å and 0 .1 Å as measured by the average distance between outermost carbons and hydrogens along the surface normal for Ti- and Sr-STO surface, respectively. The calculated STO-Graphene(CNR) distance as defined by the distance between the Graphene carbons(CNR hydrogens) and the surface top oxygen layer and adsorption energy per C atom is of 3.116/3.227(2.819/3.050 Å) and 60.0/70.0(91.0/124 meV) for the Ti/Sr-STO surface, respectively. All of these structural and energetic features have their origin in the electronic structure and this is further analysed in the next section.

3.2. Electronic structure of interfaces.

3.2.1. Graphene/TiO_2-terminated STO

Turning to the electronic structure of the Ti-STO/Graphene interface, we look first at the electronic density of states (DOS) for the Ti-STO surface, shown in Fig. 3. It is readily apparent that the DOS of the free graphene sheet (Fig. 3b) and of STO (Fig. 3c) are broadly similar to the DOS of the hybrid and that their interaction is of van der Waals (vdW) character, *i.e.* no significant modification of the electronic levels of both components. This also suggests that strain has a marginal effect on the DOS of the pure graphene and this is further supported by the relatively low calculated adsorption energy of the graphene sheet on the Ti-STO surface of 60.0 meV per C atom. Our results therefore show that the weaker TiO_2 terminated surface interaction may lead to poor adhesion of graphene. Another feature is that the graphene canonical point (where the valence band touches the conduction band) is preserved upon interaction with Ti-STO (Fig. 3b) and aligns with the conduction band minimum (CBM) of STO that is of Ti-*3d* character (Fig. 3a).

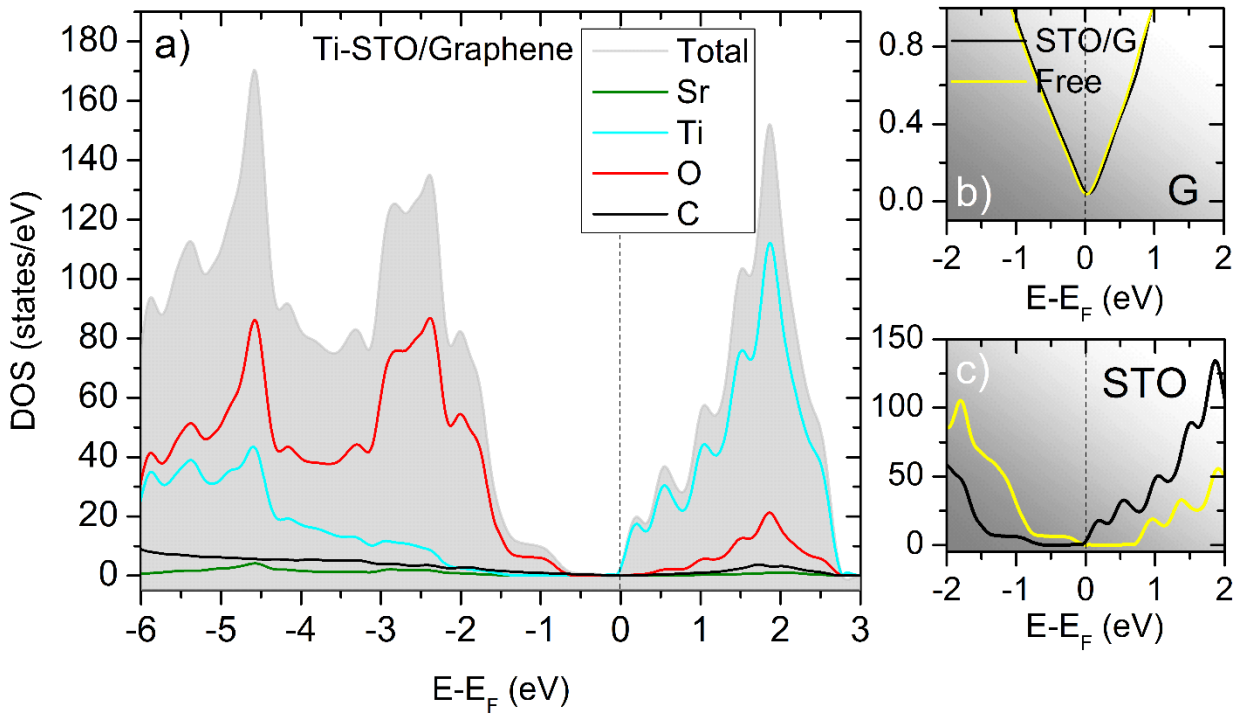

Figure 3: a) Total and atom projected DOS for the Ti-STO/Graphene interface. b) DOS near the Fermi level of graphene and Ti-STO/graphene. c) DOS near the Fermi level of the clean Ti-STO surface and the Ti-STO/Graphene interface. For all the systems Fermi level is set at 0 eV, the position of the valence band maximum.

3.2.2. Graphene/SrO-terminated STO

In contrast to Ti-terminated STO, our calculations reveal that the mechanism of interaction of the graphene sheet is radically different for Sr-terminated STO, as shown in Fig. 4. In contrast to the good electronic level alignment of graphene on the Ti-STO surface, on Sr-STO the graphene electronic levels align with the valence band maximum (VBM) of the STO surface, which is dominated by the O-*2p* contribution, Fig. 4a. This leads to a stronger interaction of the oxygen with the graphene layer than for the Ti-STO surface. This can also be seen in the modification of the STO DOS below the Fermi level as shown in Fig. 4c. This is reflected in the 20-40% higher adsorption energies calculated for the graphene sheet on Sr-STO than on Ti-STO. Although the graphene canonical point is also preserved here, it is now shifted by 0.5 eV below the Fermi level as seen in Fig. 4b, which results in an effective *n*-type doping of the graphene sheet.

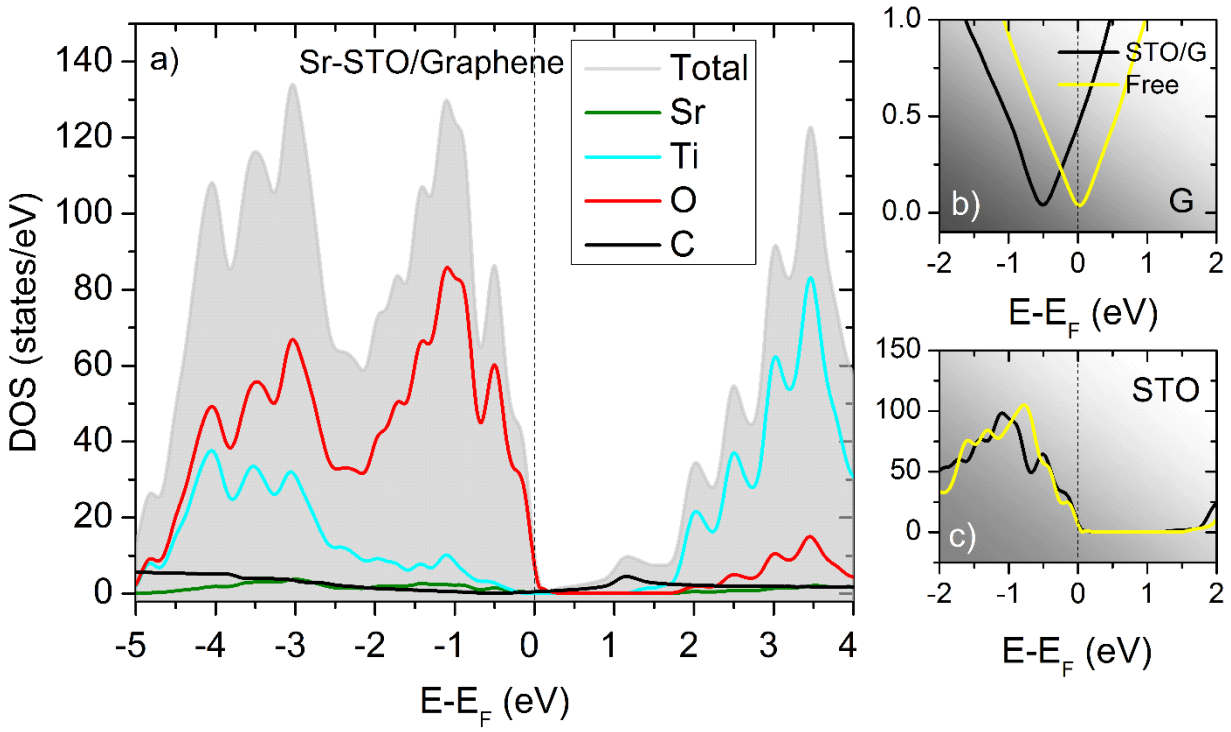

Figure 4: a) Total and species projected DOS for the Sr-STO/Graphene interface. b) DOS near the Fermi level of graphene and Sr-STO/graphene. c) DOS near the Fermi level of the clean Sr-STO surface and the Sr-STO/Graphene interface. For all the systems Fermi level is set at 0 eV, the position of the valence band minimum.

It needs to be noted that an opposite *p*-type doping of a graphene sheet on STO has been recently achieved by introduction of STO subsurface oxygen vacancies.[22] Described above the Fermi level shift of graphene can be explained by the difference in work function between the graphene and substrate that leads to electron transfer between them in order to equilibrate their Fermi levels.[36]

3.2.3. CNR/TiO_2-terminated STO.

The zigzag CNRs have previously been predicted to have a magnetic ground state with ferromagnetic ordering at each zigzag edge and antiparallel spin orientation at the two edges[18], which agrees with our calculations. Due to the edge magnetisation, a staggered sublattice potential is introduced on the hexagonal carbon lattice, and a band gap appears, see Fig. 5b. The edge-states around the Fermi level form flat bands[18] that give rise to a very large sharp DOS at the vicinity of the Fermi level as shown in Fig. 5b. Moreover, the transport properties of carbon nanoribbons are closely related to their symmetry.[37] Figure 5a shows the total and projected onto CNR atoms spin polarised DOS for Ti-STO/CNR interface (for the PDOS of the Sr, Ti and O refer to Fig. 3a and Fig. 4a above).

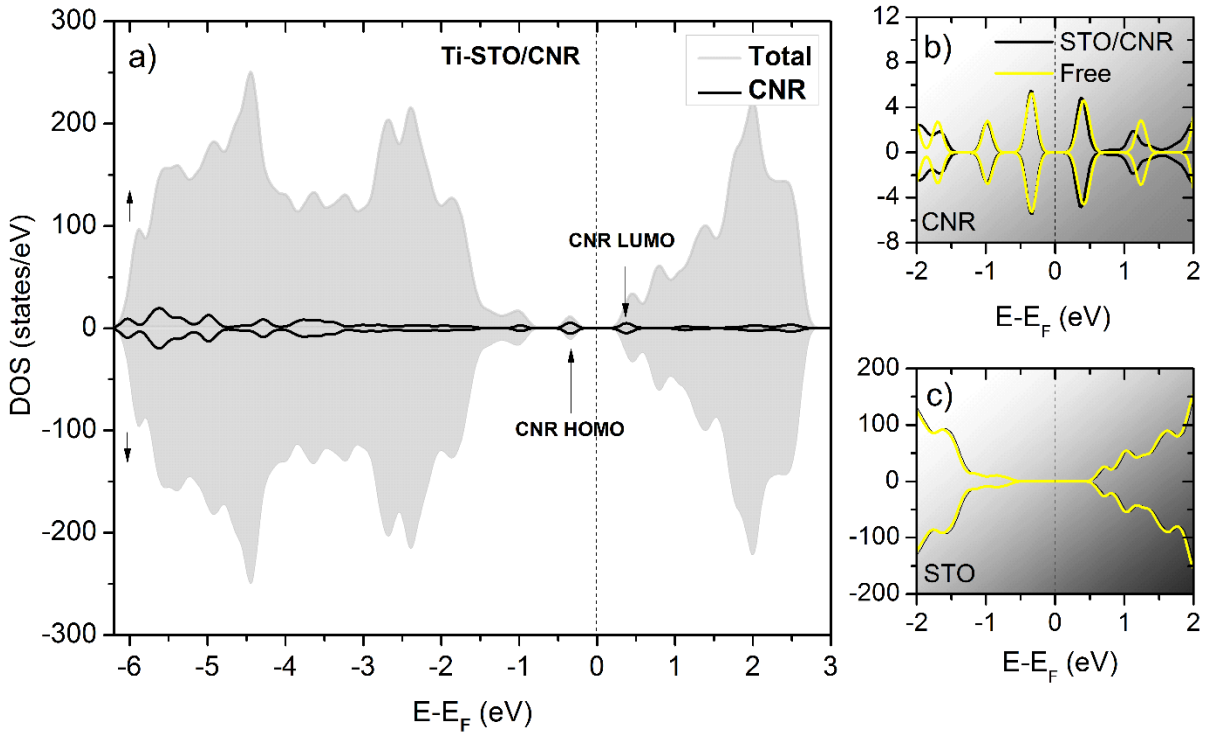

Figure 5: a) Total and projected onto CNR atoms DOS of Ti-STO/CNR interface. DOS of the Free and from the interface a) CNR and b) Ti-STO surface c) DOS near the Fermi level of the clean Ti-STO surface and from Ti-STO/CNR interface. Positions of CNR HOMO and LUMO is highlighted. Fermi level is set up in the middle of the band gap.

As can be seen from Fig. 5a, the magnetic properties of the CNR are preserved upon interaction with the Ti-STO where two spin channels are intact as in the free CNR (Fig. 5b). The comparison between DOS of the free and adsorbed CNR reveals that its electronic levels are only marginally altered by the presence of the surface (Fig. 5b-c), similar to that discussed above for the Ti-STO/graphene interface. The most interesting, aspect of this system is the electronic level alignment between CNR and STO surface. The CNR highest occupied molecular orbital (HOMO) aligns with the middle of the Ti-STO surface band gap whereas the lowest unoccupied molecular (LUMO) aligns with its CBM, as highlighted in Fig. 5a. Thus the band-gap of the Ti-STO is lowered, but the semiconducting properties of the CNR are preserved. The positioning of the CNR's HOMO charge carries in the middle of the STO band-gap resembles an *n*-type doping of STO. Therefore, such hybrid interfaces can provide a new way of decreasing a band gap and simultaneously increasing carrier concentration of an oxide. The CNR's band gap can be tuned by changing the CNR width and chirality.[18, 19] For example, it is known that the band gap of semiconducting CNRs decreases with an increase of their width.[18] Therefore, the desired modification of the material electronic properties could in principle be achieved by selectively matching

CNR with desired width/band gap to match the surface electronic properties.

3.2.4. CNR/SrO-terminated STO

The DOS of Sr-STO/CNR surface is shown in Fig. 6a-c. Similarly to the Sr-STO/Graphene, the electronic levels of the interface are significantly modified as compared to those of the free CNR (Fig. 6b) and STO surface (Fig. 6c). In contrast to the Ti-STO/CNR, the system has a metallic character and the VBM has both STO and CNR character (Fig. 6a). The new CNR states appear at the Fermi level as shown in Fig. 6b and are a result of hybridization between the electronic levels of the surface O-$2p_z$ and π orbitals of the CNR carbons, which results in a covalent bond between the CNR and Sr-STO.

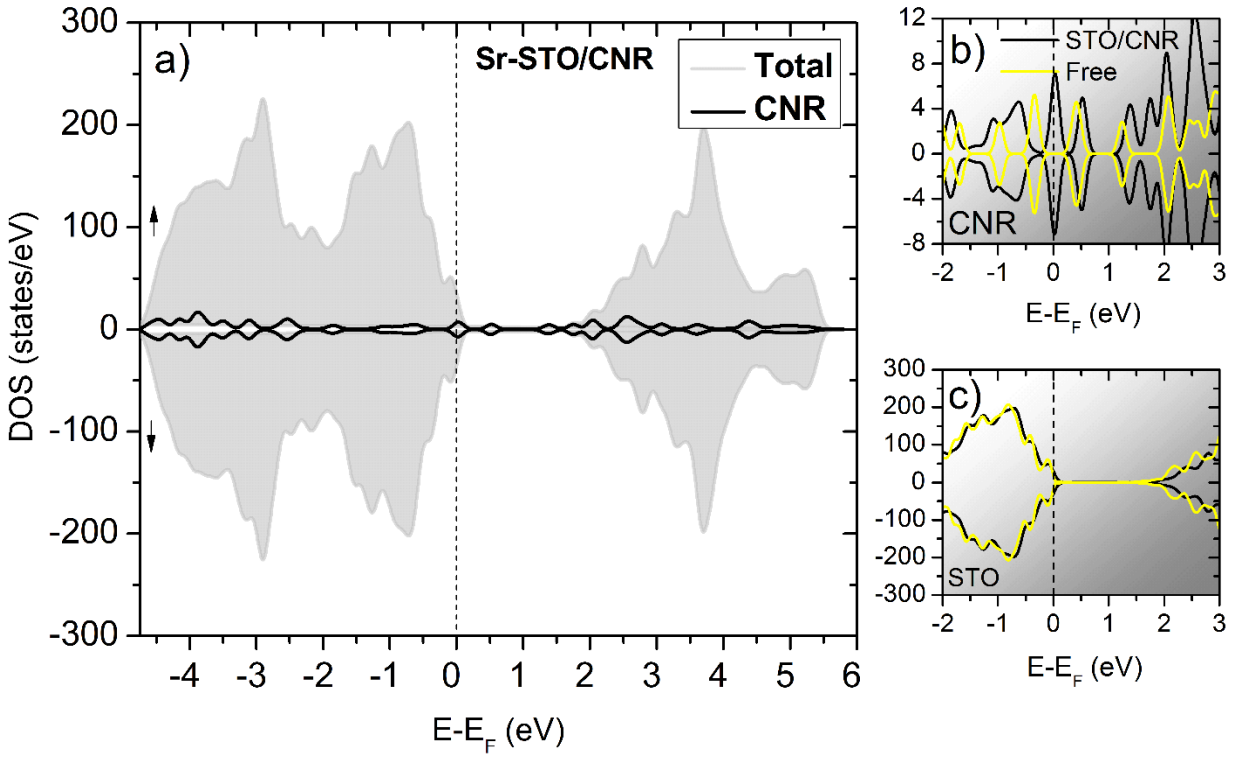

Figure 6: a) Total DOS of Sr-STO/CNR interface and projected onto CNR atoms. DOS of the Free and from the Sr-STO/CNR b) CNR and c) DOS near the Fermi level of the clean Sr-STO surface and from Sr-STO/CNR interface. The Fermi level is set up at VBM.

The alignment of the Fermi level that cuts the top VB of the Sr-STO (Fig. 6c) suggesting the system of a *p*-type character, which is confirmed by calculated positive Seebeck coefficient as discussed below. Therefore, here as well as in the STO/graphene interface, the interaction with the different termination of the STO surface leads to a change in the conductivity character, *i.e.*, *n*-type and *p*-type for the

interface with Ti-STO and Sr-STO interfaces, respectively. These changes in the electronic structure directly affect the calculated Seebeck coefficient and electronic conductivity. In the following section, we discuss the evolution of the Seebeck coefficient and electronic conductivity for these systems as a function of temperature and electronic chemical potential.

3.2.5. **Electronic transport properties of graphene/STO and CNR/STO interfaces.**

In solids, both charge and heat flows are simultaneously generated when an electrochemical potential or a temperature gradient is present, resulting in new properties. The Seebeck coefficient and electrical conductivity are determined by the band structure and electron scattering mechanisms. We find that the interaction of the graphene and CNR with the STO alters the electronic properties, the Seebeck coefficient and the electronic conductivity of the pristine ones. Figure 7 shows the calculated Seebeck coefficient as a function of electronic chemical potential and temperature as well as $\sigma*\tau^{-1}$ as a function of electronic chemical potential for the free graphene sheet and CNR as well as their interfaces with STO.

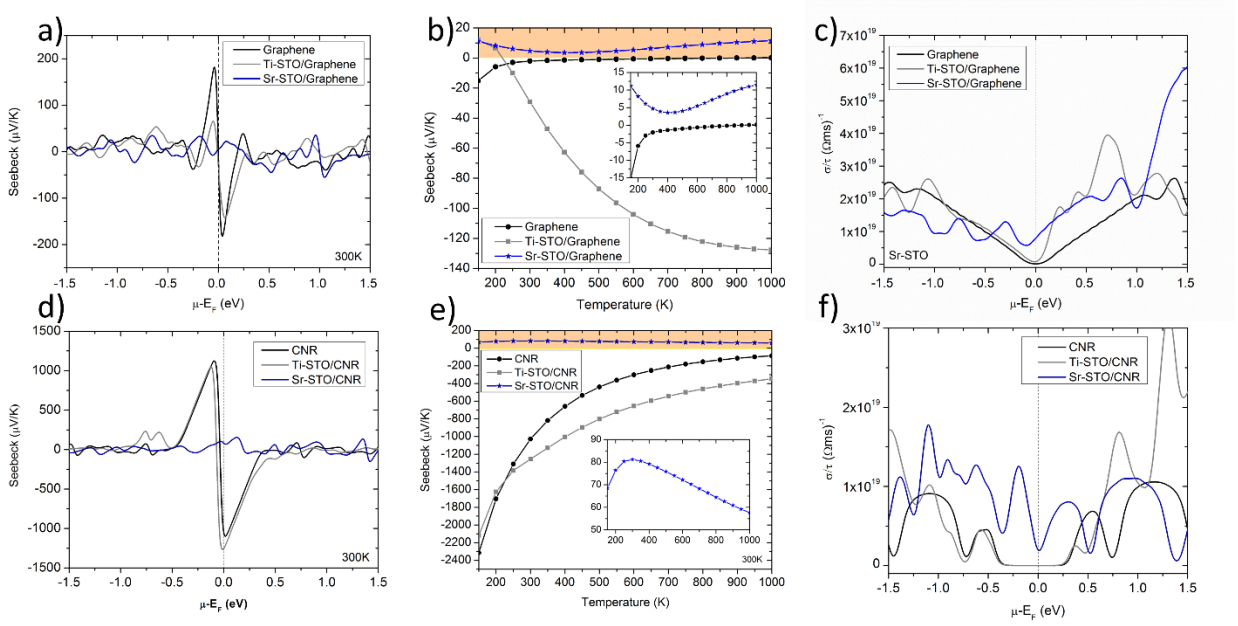

Figure 7: Calculated Seebeck coefficient as a function of a) chemical potential and b) temperature for the free graphene and Ti(Sr)-STO/Graphene interface. Calculated Seebeck coefficient as a function of d) chemical potential and e) temperature for the free CNR and Ti(Sr)-STO/CNR interface. Calculated $\sigma*\tau^{-1}$ as a function of chemical potential for c) free graphene and Ti(Sr)-STO/Graphene interface and f) free CNR and Ti(Sr)-STO/CNR interface. Highlights and insets in b) and e) show regions

where Seebeck coefficient takes positive value.

The calculated maximum absolute value of the Seebeck coefficient is 185 and 1095 μV/K for the free graphene and CNR, respectively (Fig. 7a and 7d). The 5 times increase of the Seebeck coefficient for CNR is a result of its one-dimensional structure, which introduces the sharp DOS peaks around the Fermi level as shown in Fig. 6b. This is in a qualitative agreement with the tight-binding results of Ouyang *et al.*[38] where calculated Seebeck coefficient near the Fermi level was in order of mV/K for semiconducting CNRs, whereas are in μV/K range for graphene. Looking at the evolution of the Seebeck coefficient with temperature we observe that its absolute value increases for Ti-STO/Graphene (Fig. 7b) and decrease for Ti-STO/CNR (Fig. 7e) as the temperature rises. The latter behaves as the free CNR (Fig. 7e) whereas the former in opposite way to the free graphene where it is decreasing with temperature (Fig. 7b). This shows that the Seebeck coefficient and the electronic conductivity of the hybrid material is dominated by the CNR for the Ti-STO/CNR but is of more complex form for the Ti-STO/Graphene. This is also seen in the calculated $\sigma*\tau^{-1}$ in Fig. 7c, which shows a pronounced asymmetry around the Fermi level for the Ti-STO/Graphene as compared to the free graphene, see Fig. 7c. This is a result of the electronic level alignment between the graphene and Ti-STO discussed earlier and showed in Fig. 2a. The graphene Dirac point aligns with the CBM of STO, thus DOS (and $\sigma*\tau^{-1}$) below the Fermi level of Ti-STO/Graphene behaves like from the pristine graphene sheet as its occupied states fill the former band gap of Ti-STO (Fig. 7c), whereas because of the contribution from the empty states of Ti-STO deviates above the Fermi level. With increase of the temperature and chemical potential, the charge carriers start to populate the CB, which asymmetry leads to a different behaviour of the transport properties as in the case of the free graphene sheet. The different behaviour of the Seebeck coefficient of the adsorbed CNR and graphene sheet, despite the almost identical electronic structure to their free-standing counterparts may be attributed to the functional properties of STO such as high dielectric constant that can modify to a different extent electronic environment of the CNR and graphene on STO.[20-22] The calculated Seebeck coefficient and electronic conductivity are strikingly different for the Sr-STO interface, see Fig. 7b and 7c. The Seebeck coefficient in both cases has a positive value indicating the change of the carriers from electrons to holes. Moreover due to the electronic states crossing the Fermi level that arise from the interaction between the components, the system has a metallic character. In summary the interaction of graphene and CNR with a different termination of the STO surface leads not only to the change of the conductivity type from *n*-type (Ti-STO) to *p*-type (Sr-STO) but also a change of behaviour from semiconducting to metallic as in the case of STO/CNR interface. This may have important consequences

for operation of nano-electronic devices based on such hybrid materials and guide their design.

4. Conclusions

In this work we have studied the structural, electronic and thermoelectric transport properties of the interfaces of graphene and CNR with $SrTiO_3$ (001). Our results reveal the following key points;

1) Graphene and CNR interact weakly with the TiO_2-terminated STO surface (Ti-STO) via van der Waals interactions leading to little change in the electronic structure. In contrast, both graphene and CNR chemisorb onto the SrO- terminated STO (Sr-STO) surface with higher adsorption energies of leading to significant changes in electronic structure.
2) Carbon nanoribbons has a very high calculated Seebeck coefficient that originates from its one-dimensional structure and, which preserved upon interaction with the Ti-STO surface. Moreover, such an interaction places CNR's HOMO levels in the middle of the Ti-STO band gap, which resembles *n*-type doping of the oxide.
3) Interaction of both graphene and carbon nanoribbons with Sr-STO leads to a significant modification of the electronic levels and leads to a *p*-type electronic conductivity. Although the magnitude much lower than the *n*-type doping at the Ti-STO interface.

Our results show that it is possible to control the nature of the electronic conductivity of a hybrid thermoelectric system by optimizing the interface surfaces between different surface terminations.

5. Acknowledgments

This work was funded by EPSRC Programme grants EP/ K016288/1 and EP/I03601X/1. Computations were run on ARCHER through the Materials Chemistry Consortium funded by EPSRC grant number EP/L000202 and the STFC Hartree Centre (Daresbury Laboratory, U.K.) High Performance Computing facilities. Part of this work is funded by "Materials Research by Information Integration" Initiative (MI2I) project of the Support Program for Starting Up Innovation Hub from the Japan Science and Technology Agency (JST).

6. References

(1) Kovalevsky, A. V.; Yaremchenko, A. A.; Populoh, S.; Thiel, P.; Fagg, D. P.; Weidenkaff, A.; Frade, J. R., Towards a high thermoelectric performance in rare-earth substituted SrTiO3: effects provided by strongly-reducing sintering conditions. *Phys. Chem. Chem. Phys.* **2014,** 16, 26946-26954.

(2) Snyder, G. J.; Toberer, E. S., Complex thermoelectric materials. *Nat. Mater.* **2008,** 7, 105-114.

(3) Biswas, K.; He, J.; Blum, I. D.; Wu, C.-I.; Hogan, T. P.; Seidman, D. N.; Dravid, V. P.; Kanatzidis, M. G., High-performance bulk thermoelectrics with all-scale hierarchical architectures. *Nature* **2012,** 489, 414-418.

(4) Dresselhaus, M. S.; Chen, G.; Tang, M. Y.; Yang, R. G.; Lee, H.; Wang, D. Z.; Ren, Z. F.; Fleurial, J. P.; Gogna, P., New Directions for Low-Dimensional Thermoelectric Materials. *Adv. Mater.* **2007,** 19, 1043-1053.

(5) Wan, C.; Gu, X.; Dang, F.; Itoh, T.; Wang, Y.; Sasaki, H.; Kondo, M.; Koga, K.; Yabuki, K.; Snyder, G. J.; Yang, R.; Koumoto, K., Flexible n-type thermoelectric materials by organic intercalation of layered transition metal dichalcogenide TiS2. *Nat. Mater.* **2015,** 14, 622-627.

(6) Chen, Y.; Jayasekera, T.; Calzolari, A.; Kim, K. W.; Nardelli, M. B., Thermoelectric properties of graphene nanoribbons, junctions and superlattices. *J. Phys. Condens. Matter* **2010,** 22, 372202.

(7) Srivastava, D.; Norman, C.; Azough, F.; Schafer, M. C.; Guilmeau, E.; Kepaptsoglou, D.; Ramasse, Q. M.; Nicotra, G.; Freer, R., Tuning the thermoelectric properties of A-site deficient SrTiO3 ceramics by vacancies and carrier concentration. *Phys. Chem. Chem. Phys.* **2016,** 18, 26475-26486.

(8) Lin, Y.; Norman, C.; Srivastava, D.; Azough, F.; Wang, L.; Robbins, M.; Simpson, K.; Freer, R.; Kinloch, I. A., Thermoelectric Power Generation from Lanthanum Strontium Titanium Oxide at Room Temperature through the Addition of Graphene. *ACS Appl. Mater. Interfaces* **2015,** 7, 15898-15908.

(9) Novoselov, K. S.; Geim, A. K.; Morozov, S. V.; Jiang, D.; Zhang, Y.; Dubonos, S. V.; Grigorieva, I. V.; Firsov, A. A., Electric Field Effect in Atomically Thin Carbon Films. *Science* **2004,** 306, 666-669.

(10) Seol, J. H.; Jo, I.; Moore, A. L.; Lindsay, L.; Aitken, Z. H.; Pettes, M. T.; Li, X.; Yao, Z.; Huang, R.; Broido, D.; Mingo, N.; Ruoff, R. S.; Shi, L., Two-Dimensional Phonon Transport in Supported Graphene. *Science* **2010,** 328, 213-216.

(11) Zuev, Y. M.; Chang, W.; Kim, P., Thermoelectric and Magnetothermoelectric Transport Measurements of Graphene. *Phys. Rev. Lett.* **2009,** 102, 096807.

(12) Balandin, A. A., Thermal properties of graphene and nanostructured carbon materials. *Nat. Mater.* **2011,** 10, 569-581.

(13) Balandin, A. A.; Ghosh, S.; Bao, W.; Calizo, I.; Teweldebrhan, D.; Miao, F.; Lau, C. N., Superior Thermal Conductivity of Single-Layer Graphene. *Nano Lett.* **2008,** 8, 902-907.

(14) Dorgan, V. E.; Behnam, A.; Conley, H. J.; Bolotin, K. I.; Pop, E., High-Field Electrical and Thermal Transport in Suspended Graphene. *Nano Lett.* **2013,** 13, 4581-4586.

(15) Kim, J. Y.; Grossman, J. C., High-Efficiency Thermoelectrics with Functionalized Graphene. *Nano Lett.*

2015, 15, 2830-2835.

(16) Chen, X.-K.; Xie, Z.-X.; Zhou, W.-X.; Tang, L.-M.; Chen, K.-Q., Phonon wave interference in graphene and boron nitride superlattice. *Appl. Phys. Lett.* **2016,** 109, 023101.

(17) Yeandel, S. R.; Molinari, M.; Parker, S. C., Nanostructuring perovskite oxides: the impact of SrTiO3 nanocube 3D self-assembly on thermal conductivity. *RSC Adv.* **2016,** 6, 114069-114077.

(18) Son, Y.-W.; Cohen, M. L.; Louie, S. G., Energy Gaps in Graphene Nanoribbons. *Phys. Rev. Lett.* **2006,** 97, 216803.

(19) Barone, V.; Hod, O.; Scuseria, G. E., Electronic Structure and Stability of Semiconducting Graphene Nanoribbons. *Nano Lett.* **2006,** 6, 2748-2754.

(20) Couto, N. J. G.; Sacépé, B.; Morpurgo, A. F., Transport through Graphene on $SrTiO_3$. *Phys. Rev. Lett.* **2011,** 107, 225501.

(21) Park, J.; Kang, H.; Kang, K. T.; Yun, Y.; Lee, Y. H.; Choi, W. S.; Suh, D., Voltage Scaling of Graphene Device on SrTiO3 Epitaxial Thin Film. *Nano Lett.* **2016,** 16, 1754-1759.

(22) Kang, K. T.; Kang, H.; Park, J.; Suh, D.; Choi, W. S., Quantum Conductance Probing of Oxygen Vacancies in $SrTiO_3$ Epitaxial Thin Film using Graphene. *Adv. Mater.* **2017,** 29, 1700071

(23) Gogoi, P. K.; Trevisanutto, P. E.; Yang, M.; Santoso, I.; Asmara, T. C.; Terentjevs, A.; Della Sala, F.; Breese, M. B. H.; Venkatesan, T.; Feng, Y. P.; Loh, K. P.; Neto, A. H. C.; Rusydi, A., Optical conductivity renormalization of graphene on $SrTiO_3$ due to resonant excitonic effects mediated by Ti-3d orbitals. *Phys. Rev. B* **2015,** 91, 035424.

(24) Eglitis, R. I.; Vanderbilt, D., First-principles calculations of atomic and electronic structure of $SrTiO_3$ (001) and (011) surfaces. *Phys. Rev. B* **2008,** 77, 195408.

(25) Kresse, G.; Hafner, J., Ab initio molecular dynamics for liquid metals. *Phys. Rev. B* **1993,** 47, 558-561.

(26) Kresse, G.; Hafner, J., Ab initio molecular-dynamics simulation of the liquid-metal–amorphous-semiconductor transition in germanium. *Phys. Rev. B* **1994,** 49, 14251-14269.

(27) Kresse, G.; Furthmüller, J., Efficiency of ab-initio total energy calculations for metals and semiconductors using a plane-wave basis set. *Comput. Mater. Sci.* **1996,** 6, 15-50.

(28) Blöchl, P. E., Projector augmented-wave method. *Phys. Rev. B* **1994,** 50, 17953-17979.

(29) Perdew, J. P.; Burke, K.; Ernzerhof, M., Generalized Gradient Approximation Made Simple. *Phys. Rev. Lett.* **1996,** 77, 3865-3868.

(30) Grimme, S., Semiempirical GGA-type density functional constructed with a long-range dispersion

correction. *J. Comput. Chem.* **2006,** 27, 1787-1799.

(31) Madsen, G. K. H.; Singh, D. J., BoltzTraP. A code for calculating band-structure dependent quantities. *Comput. Phys. Commun.* **2006,** 175, 67-71.

(32) Muley, S. V.; Ravindra, N. M., Thermoelectric Properties of Pristine and Doped Graphene Nanosheets and Graphene Nanoribbons: Part I. *JOM* **2016,** 68, 1653-1659.

(33) Molinari, M.; Tompsett, D. A.; Parker, S. C.; Azough, F.; Freer, R., Structural, electronic and thermoelectric behaviour of CaMnO3 and $CaMnO_{(3-\delta)}$. *J. Mater. Chem. A* **2014,** 2, 14109-14117.

(34) Baran, J. D.; Molinari, M.; Kulwongwit, N.; Azough, F.; Freer, R.; Kepaptsoglou, D.; Ramasse, Q. M.; Parker, S. C., Tuning Thermoelectric Properties of Misfit Layered Cobaltites by Chemically Induced Strain. *J. Phys. Chem. C* **2015,** 119, 21818-21827.

(35) Baran, J. D.; Kepaptsoglou, D.; Molinari, M.; Kulwongwit, N.; Azough, F.; Freer, R.; Ramasse, Q. M.; Parker, S. C., Role of Structure and Defect Chemistry in High-Performance Thermoelectric Bismuth Strontium Cobalt Oxides. *Chem. Mater.* **2016,** 28, 7470-7478.

(36) Giovannetti, G.; Khomyakov, P. A.; Brocks, G.; Karpan, V. M.; van den Brink, J.; Kelly, P. J., Doping Graphene with Metal Contacts. *Phys. Rev. Lett.* **2008,** 101, 026803.

(38) Ouyang, Y.; Guo, J., A theoretical study on thermoelectric properties of graphene nanoribbons. *Appl. Phys. Lett.* **2009,** 94, 263107.

TOC

Hybrid Materials